Pharmaceutical Research, Vol. 10, No. 12, 1993

Research Article

Transport of Ionic Species in Skin: Contribution of Pores to the Overall Skin Conductance

Erik R. Scott,[1,2] Ana I. Laplaza,[1,3] Henry S. White,[1,4] and J. Bradley Phipps[5]

Received March 30, 1993; accepted July 3, 1993

Two methods are reported that allow visualization of high conductance paths in skin at current densities typically used during clinical iontophoretic drug delivery (10–200 $\mu A/cm^2$). In the first method, the counter-directional iontophoretic transport of $Fe(CN)_6^{4-}$ and Fe^{3+} across skin results in the precipitation of colloidal prussian blue, $Fe_4[Fe(CN)_6]_3$, at sites of high iontophoretic flux. The appearance of localized deposits of $Fe_4[Fe(CN)_6]_3$ is recorded by video microscopy and used to document the activation of low-resistance paths. In the second method, the ionic flux of $Fe(CN)_6^{4-}$ through pores is directly imaged by scanning electrochemical microscopy (SECM). Both methods demonstrate that the iontophoretic flux across skin is highly localized. Activation of low-resistance pores in hairless mouse skin is shown to occur during iontophoresis. The spatial density of current carrying pores increases from 0 to 100–600 pores/cm^2 during the first 30–60 min of iontophoresis. At longer times, the active pore density approaches a quasi-steady-state value that is proportional to the applied current density. The total conductance of the skin is proportional to the number of pores, consistent with a model of conduction in skin that is comprised of low-resistivity pores in parallel with a high-resistivity bulk phase. The contribution of pores to the total skin conductance during iontophoresis increases from an initial value of 0–5% to a quasi-steady-state value of 50–95%.

KEY WORDS: iontophoresis; electrotransport; hairless mouse; skin resistance; shunt pathways; scanning electrochemical microscopy.

INTRODUCTION

Knowledge of the electrical properties of skin is important in the area of electrofacilitated transcutaneous drug transport (iontophoresis). The skin has been modeled electrically as a parallel resistor and capacitor, in series with a second resistor (1–4). The value of the series resistance is low compared to that of the parallel resistor, such that the parallel resistor/capacitor element dominates the skin impedance at low frequencies. Removal of skin's outer layer, the stratum corneum, has been shown effectively to eliminate the parallel resistance, leading to the conclusion that the dominant parallel resistive component is located exclusively in the stratum corneum (2). Thus, it is generally accepted that the stratum corneum is the major barrier to iontophoretic transport (5).

Homogeneous models of membrane permeability have proven unsatisfactory for describing iontophoretic transport across skin, and the importance of skin appendages (e.g., hair follicles, sweat ducts) as low-resistance shunt pathways through which ions traverse the skin has been the subject of debate for decades (6). It is generally agreed that skin appendages can provide low-resistivity channels across the otherwise highly resistive stratum corneum. We use the terms "pore" and "shunt" to denote a local, high-conductance pathway, without making presumptions about the physiological nature of such a structure. Experimental results, based on staining of pores during iontophoresis of charged dyes, as well as using potentiometric microelectrodes to measure electric field gradients, have shown that appendages are associated with regions of high current density (7–11). However, the small size and spatial density of appendages have prevented quantitative determination of the contribution of shunt paths to the overall conductance of skin (12–17).

During iontophoresis, the dc resistance of skin (R_s) is a function of time and the magnitude of the applied current (18). Typically, R_s decreases rapidly during the initial ~10 min of iontophoresis and gradually levels off to a quasi-steady-state value. Because of this effect, the skin's current/voltage response, while apparently ohmic at any given instant during iontophoresis, cannot be described by constant-valued electrical circuit components. While previous works have shown that the stratum corneum is chiefly responsible for skin's high resistance and that the resistance of this layer changes in time, there is a need to address what changes

[1] Department of Chemical Engineering and Materials Science, University of Minnesota, Minneapolis, Minnesota 55455.
[2] Present address: Medtronic, Inc., Brooklyn Center, Minnesota.
[3] Present address: Department of Chemical Engineering, Massachusetts Institute of Technology, Cambridge, Massachusetts 02139.
[4] To whom correspondence should be addressed at Department of Chemistry, Henry Eyring Building, University of Utah, Salt Lake City, Utah 84112.
[5] Alza Corporation, Spring Lake Park, Minnesota.

0724-8741/93/1200-1699$07.00/0

occur within this layer which are responsible for the decrease in resistance.

We report on studies of iontophoresis through hairless mouse skin. The hairless mouse has been commonly used as a model for transcutaneous transport (19). Although mature hairless mice have few hairs (as the name suggests), the presence of several hundred hair follicles per square centimeter allows the use of this animal model to study whether such follicles behave as shunt pathways. Our experiments involved simultaneous measurements of the dc skin resistance and the number of shunt pathways during iontophoretic and passive transport of ferrocyanide [$Fe(CN)_6^{4-}$] across hairless mouse skin. The current densities used in our transport studies (10–200 $\mu A/cm^2$) are commonly used in iontophoretic drug delivery (20–24). Scanning electrochemical microscopy (SECM) and video microscopy are used to document the activation of shunt pathways during iontophoresis. By monitoring the number of pores present and the overall skin conductance over time, both the conductance of individual pores and the relative contribution of pores to the overall conductance of skin are quantitatively assessed. During iontophoresis, the resistance of skin is inversely correlated with both time and magnitude of current. It is shown that both of these phenomena can be attributed to an increased number of high-conductance shunt pathways across the stratum corneum.

MATERIALS AND METHODS

The experimental apparatus shown in Fig. 1 performs four distinct functions used in analyses of iontophoretic currents: (i) a constant current across skin samples is supplied by the galvanostat and two large-area Ag/AgCl electrodes; (ii) the electrical resistance of skin is measured by the four-point probe method using the two saturated calomel reference electrodes (SCE) as voltage-measuring electrodes; (iii) the deposition of Prussian blue dye on the skin surface is monitored during iontophoresis using a videocamera and telephoto lens; and (iv) ion transport rates through individual pores are measured quantitatively by a scanning electrochemical microscope. All experiments were made at ambient room temperature. Details of the instrumental components that perform each function are described below.

A disk-shaped area of skin separates the solutions in the donor (lower) and receptor (upper) compartments (Fig. 1) of a custom-built Teflon iontophoresis cell. A glass window is mounted at the top of the receptor compartment for optical imaging of skin by video microscopy. Ports in the diffusion cell provide connections to SCEs and Ag/AgCl current-driving electrodes. Glass frits are used to separate the Ag/AgCl electrodes from the main compartments of the cell. A detailed description of the cell construction and the specimen mounting procedure are given in Ref. 11.

Skin Samples. Skin was removed from the back and sides of freshly sacrificed hairless mice (male, age 7–12 weeks, Charles River, strain SKH-1). The loosely attached subcutaneous brown fat was removed by gentle rubbing with a damp gauze sponge. Skin samples were placed between layers of sterile saline-soaked gauze and stored in a refrigerator until use. Storage times ranged from 2 to 80 hr. Disk-shaped areas of skin (0.50 cm^2) were exposed to test solutions in the iontophoresis cell, with the epidermal side facing the upper (receptor) compartment.

Scanning Electrochemical Microscopy (SECM). A microelectrode, prepared by deposition of platinum at the end of an 8-μm-diameter carbon fiber, is used to measure the concentration of an electroactive species as it emerges from the skin (Fig. 1). The potential of the microelectrode is biased, using a potentiostat, at a constant value which is sufficiently positive (or negative) to oxidize (or reduce) the electroactive species at the mass transport-controlled rate. In the investigations reported below, which are concerned with imaging the local pathways of $Fe(CN)_6^{4-}$ transport in skin, the microelectrode is poised at 0.4–0.5 V vs a saturated calomel electrode (SCE). At such a potential, the oxidation of $Fe(CN)_6^{4-}$ at the Pt tip, Eq. (1), is diffusion limited.

$$Fe(CN)_6^{4-} \rightarrow Fe(CN)_6^{-3} + e^-, \qquad E^{0'} = 0.185 \text{ vs SCE} \tag{1}$$

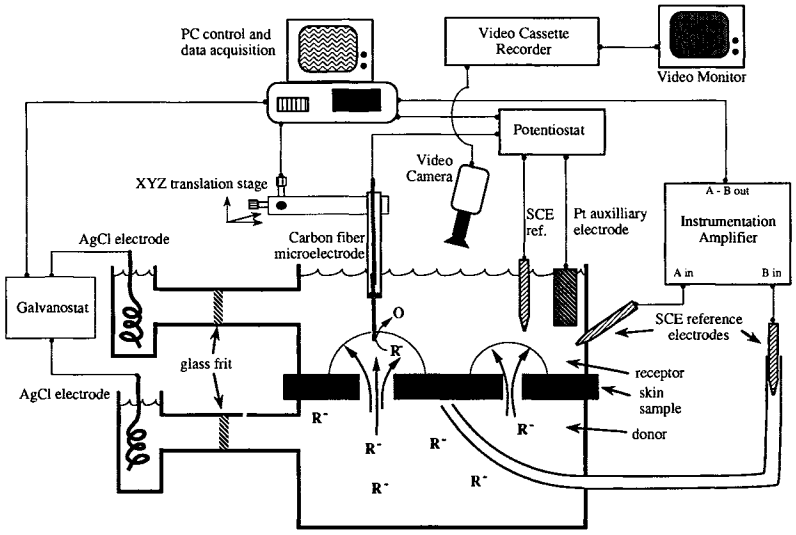

Fig. 1. Schematic diagram of scanning electrochemical microscope (SECM) and iontophoresis cell.

$E^{0'}$ is the standard redox potential of the $Fe(CN)_6^{4-}/Fe(CN)_6^{3-}$ redox couple. The current measured at the Pt tip (i_t) is proportional to the local concentration, $C(x,y,z)$, of $Fe(CN)_6^{4-}$ by the relationship

$$i_t = 4nFDC(x,y,z)r_t \quad (2)$$

where n = 1 Eq/mol, F = 96487 C/eq, D is the diffusion constant of $Fe(CN)_6^{4-}$ ($\sim 7 \times 10^{-6}$ cm^2/sec), and r_t is the radius of the Pt tip (4 μm).

SECM is used in our studies (i) to obtain qualitative images of the local concentration of $Fe(CN)_6^{4-}$ at the skin/receptor compartment interface and (ii) to measure quantitatively the rate of mass transport of $Fe(CN)_6^{4-}$ through individual pores. In the imaging mode, the Pt microelectrode is rastered across the skin surface at a constant height z, ranging between 5 and 20 μm, while maintaining its potential at 0.5 V vs SCE. Motion of the tip in the x and y directions is controlled using piezoelectric inchworm microtranslation stages (Fig. 1). From Eq. (1), the current measured at the tip is proportional to the local concentration at fixed z, $C(x,y)$. Thus, since a high local value of $C(x,y)$ implies a source of $Fe(CN)_6^{4-}$, regions where i_t is large correspond to a localized high flux of $Fe(CN)_6^{4-}$ across skin. Greyscale plots of $C(x,y)$ are used to determine the x,y position of pores in the skin where the $Fe(CN)_6^{4-}$ flux is large.

In the second application of SECM, the current measured at the microelectrode is used to determine quantitatively the rate of transport of $Fe(CN)_6^{4-}$ through individual pores. To accomplish this, i_t is measured at different vertical heights, z, while rastering the microelectrode in the x,y plane. Thus, the concentration of $Fe(CN)_6^{4-}$ is measured throughout a volume element of the solution directly above the pore. Isoconcentration lines connecting x,y,z points in space where $C(x,y,z)$ has a constant value are constructed from the data. Because the pores in skin have microscopic dimensions, the flux of $Fe(CN)_6^{4-}$ from the pores is radially divergent, resulting in hemisphere-shaped isoconcentration surfaces. The radius of the hemispherical isoconcentration line (r_{hs}) is obtained by a least-squares fit to the data. The rate of mass transport (J_p) of $Fe(CN)_6^{4-}$ through a pore is calculated from r_{hs} and the value of $C(x,y,z)$ along the isoconcentration line, as indicated by Eq. (3).

$$J_p = 2\pi C(x,y,z)Dr_{hs} \quad (3)$$

Equation (3) has been used in SECM analysis to determine the flux through pores in synthetic membranes and in skin (25).

Measurement of Skin Resistance. The dc resistance (R_s) of skin samples was measured using a four-electrode method. An applied current (i_{app}) was passed between the two Ag/AgCl electrodes by means of a galvanostat (RDE-4, Pine Instruments, Grove City, PA). The transmembrane potential (V_s) was measured as the potential difference between an SCE in the receptor compartment and another SCE in contact with the donor compartment via a ~25-cm length of ¼-in.-i.d. PVC tubing. The ohmic (i–R) potential drop across this length of tubing was negligible. The voltage between the two SCE reference electrodes was measured with an instrumentation amplifier (MOS-FET op amps, Type CA-3140) which had an input impedance $>10^{15}$ Ω. The skin resistance was determined from the slope of a plot of V_s vs i_{app}. An IBM XT computer, with a combined digital-analog/analog-digital interface (Data Translation, Model DT-2805), was used to control i_{app} and V_s measurement functions.

The skin resistance was periodically measured during iontophoresis experiments. In these measurements, the constant iontophoretic current was interrupted and V_s was recorded as a function of i_{app} while decreasing i_{app} in a stepwise fashion from an initial value (i_0). Resistance was calculated from linear least-squares slopes of plots of V_s vs i_{app}. The value of i_0 chosen for the resistance measurement was equal to the value of the constant iontophoretic current prior to the resistance measurements, except during experiments involving passive transport. In the latter experiments, a maximum value of 10 μA was used for i_0. The relaxation time constant for the parallel RC component of the equivalent circuit for human and guinea pig skin is of the order of 10^{-4} sec (1,26,27). Thus, after each stepwise change in i_{app}, the measurement of V_s was delayed by 1.0 sec to allow the V_s to attain a new steady value. After this 1-sec delay, V_s was sampled at an approximate rate of 100 samples/sec and signal averaged over a period of 0.5 sec. Over the time scale of the measurement of R_s (<10 sec), the skin was found to have an ohmic response for all current densities studied (0–200 μA/cm^2).

Histological Preparation of Samples. Two standard histological preparation techniques were used to obtain thin horizontal serial sections for optical microscopy. Samples which had been fixed in a glutaraldehyde solution were dehydrated and embedded in wax. Unfixed samples were imbedded and frozen at −25°C. Serial thin sections (4–16 μm) were cut from both types tissue block and were mounted on glass slides. Because the epidermis of hairless mouse skin was very thin (~30 μm), the horizontal sections were obtained primarily from the dermis. Control specimens and some PB-stained specimens were stained with eosin and hematoxylin.

Preparation of Solutions. All chemicals were used as received and were ACS reagent grade or higher. Water (18 MΩ) was purified using either a Water Prodigy (Labconco, Kansas City, MO) or an E Pure (Barnestad, Dubuque, IA) system. The donor solution contained 0.1 *M* $K_4Fe(CN)_6$ (unbuffered, pH ~8.1) in all experiments except during the measurement of ferric ion transference number. Receptor solutions contained either 0.1 *M* NaCl (pH ~6.1) or a mixture of 0.01 *M* $FeCl_3$/0.1 *M* NaCl (pH ~2.2).

Spectroscopic Analysis. The transference numbers of $Fe(CN)_6^{4-}$ and Fe^{3+} were determined by inductively coupled plasma–mass spectroscopic (ICP-MS) analysis of ^{54}Fe and ^{57}Fe concentrations in solutions drawn from the receptor compartment. Commercially available calibration standards, consisting of Fe dissolved in 5% HNO_3, were used (Johnson Matthey, Ward Hill, MA, or VHG Labs, Manchester, NH).

Prussian Blue Deposition. Simultaneous iontophoretic transport of Fe^{3+} and $Fe(CN)_6^{4-}$ across skin resulted in the deposition of colloidal Prussian blue (PB) on the skin. In these experiments, the donor (dermal side) and receptor (epidermal side) compartments of the iontophoresis cell contain aqueous solutions of $Fe(CN)_6^{4-}$ and Fe^{3+}, respectively. The donor compartment is located below the skin sample and contacts the dermal side of skin. The receptor compart-

ment is located above the skin sample and contacts the epidermal side of skin (Fig. 1). Electromigration of ions occurs when a current is applied across the skin. Because the species have opposite charges and are on opposite sides of the skin, both species are driven across the skin, when an anodic current is applied to the Ag/AgCl electrode in the receptor compartment. We refer to this process as counter-directional iontophoresis. Insoluble, colloidal PB (chemical formula: $Fe_4[Fe(CN)_6]_3$) forms upon complexation of $Fe(CN)_6^{4-}$ and Fe^{3+}. Thus, PB deposition serves to mark areas of high ion flux. Because the rate of transport of $Fe(CN)_6^{4-}$ through skin is several orders of magnitude greater than that of Fe^{3+} (*vide infra*), almost all of the dye is formed and deposited at the interface between the skin and the receptor compartment. A similar PB technique for marking pores in skin during passive and iontophoretic transport experiments has been reported (13,28), but our technique is most similar to a "countercurrent" method used to deposit PB in ion-exchange membranes (29).

PB accumulated on the surface of the stratum corneum in discrete, quasi-circular areas with diameters ranging from 40 to 200 μm. As discussed below, each region of deposition corresponds to a single current-carrying pore. Video microscopy was used to document the formation of PB on the skin during iontophoresis.

RESULTS AND DISCUSSION

Observation of Porous Pathways. Localized regions of high ionic flux across skin samples were detected by simultaneous iontophoretic transport of $Fe(CN)_6^{4-}$ (in the donor compartment) and Fe^{3+} (in the receptor compartment). Since insoluble PB is formed by complexation of Fe^{3+} and $Fe(CN)_6^{4-}$, sites of accumulation of this blue dye, either within or on the skin, indicate regions that correspond to locally high rates of ionic flux.

Figure 2 shows the temporal evolution of a PB dot pattern on skin during 2 hr of iontophoresis at 40 μA/cm^2. After passing current for a few minutes, several dark blue dots appear on the upper (epidermal) surface, indicating a high ion flux through discrete pathways. Continuous iontophoresis of $Fe(CN)_6^{4-}$ and Fe^{3+} resulted in an increase in the number of PB dots with time, indicating that the number of pores that act as regions of high ionic flux increases. For the experiment shown in Fig. 2, the number of PB dots increased from a value of 0 at time $t = 0$ min to 12 at 15 min, 85 at 30 min, 130 at 1 hr, and 170 at the end of the experiment (2 hr). In a later section, we show that the number of PB dots correlates with the measured resistance of the skin sample.

No significant amount of PB was deposited within the skin as indicated by inspection of horizontal thin sections of PB treated skin. Rather, the majority of PB formed in the aqueous receptor compartment just above the stratum corneum surface. To explain this effect, we measured the transference number of $Fe(CN)_6^{4-}$ and Fe^{3+} in skin independently, to determine the relative transport rates of each ion. In separate experiments, 0.1 *M* $K_4Fe(CN)_6$ or 0.01 *M* $FeCl_3$/0.1 *M* NaCl was placed in the donor compartment of the iontophoresis cell. In each case the receptor compartment contained 0.1 *M* NaCl. When $FeCl_3$ was used, the pH of the receptor was adjusted to pH 2.1 by the addition of HCl in

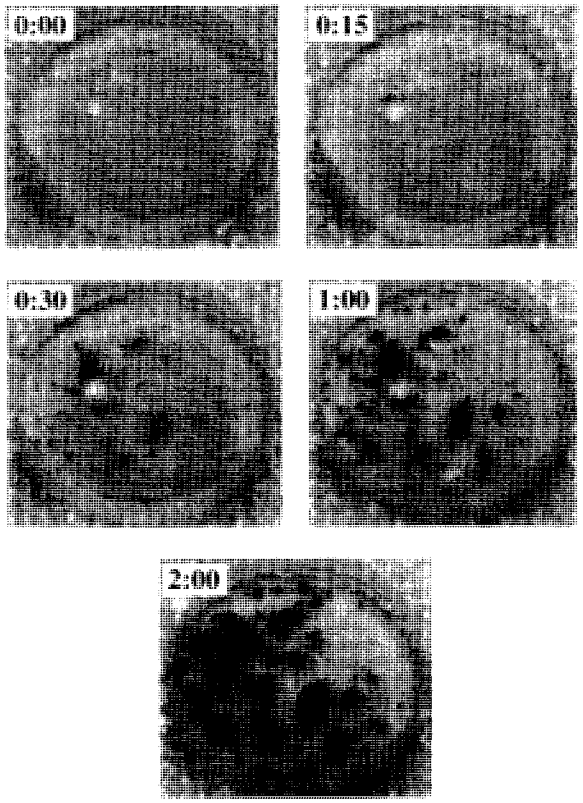

Fig. 2. Video images of hairless mouse skin during iontophoresis of $Fe(CN)_6^{4-}$ and Fe^{3+}. The dark dots correspond to the localized deposition of PB dye at pore openings. Applied current density: 40 μA/cm^2. Image area is approx. 9 × 9 mm. Donor solution: 0.1 *M* $K_4Fe(CN)_6$ (pH ~8.1). Receptor: 0.01 *M* $FeCl_3$/0.1 *M* NaCl (pH ~2.2).

order to prevent formation of $Fe(OH)_3$. In both experiments, current densities of 40 μA/cm^2 were passed. Receptor solutions were collected after at least 3 hr, and samples were analyzed for Fe concentration by ICP-MS. The transport rate N (mol/sec) was determined for each species from the concentration analysis and was used to compute the transference number (t_d) by Eq. (4).

$$t_d = \frac{|z|FN}{i_{app}} \tag{4}$$

In Eq. (4), z is the charge of each species and F is Faraday's constant (96487 C/eq). Transference numbers of 0.3 and 2×10^{-4} were obtained for $Fe(CN)_6^{4-}$ and Fe^{3+}, respectively, indicating that $Fe(CN)_6^{4-}$ traversed the skin at a rate several orders of magnitude greater than that of Fe^{3+}. The reader should be aware that one of the reasons for such a small observed transference number of Fe^{3+} is that there was 0.1 *M* NaCl in addition to the 0.01 *M* $FeCl_3$ in the donor compartment: the presence of Na^+ as a coion with Fe^{3+} resulted in a decrease in the Fe^{3+} transference number. Thus, during counter-directional iontophoresis of both the Fe^3 and the $Fe(CN)_6^{4-}$, the majority of PB collects at the skin/receptor compartment interface, as schematically illustrated in Fig. 3.

It was important to know whether the conditions of the PB experiments caused significant alteration of normal transport mechanisms in the skin samples. To explore pos-

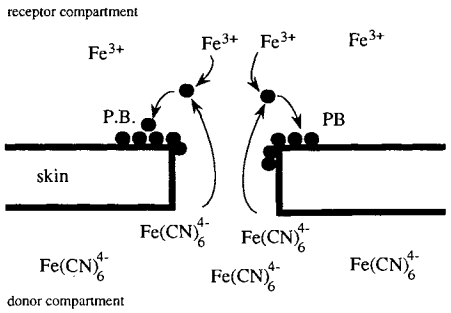

Fig. 3. Schematic representation of the precipitation of PB due to mixing of $Fe(CN)_6^{4-}$ and Fe^{3+} near a pore opening. PB forms primarily at the skin/receptor compartment interface, due to high transdermal flux of $Fe(CN)_6^{4-}$ relative to that of Fe^{3+}.

sible effects of PB deposition on the number and conductance of individual pores, SECM was used to measure quantitatively the ion flux through several pores, before and after Prussian blue formation. In these measurements, SECM was initially used to image a region of a skin sample and locate several pores. The receptor compartment contained 0.1 *M* NaCl (pH ~6.1) during the SECM measurements. Figure 4A shows a SECM image of a 1 × 1-mm area of hairless mouse skin during iontophoresis of $Fe(CN)_6^{4-}$ across the skin sample at 40 μA/cm². The bright region corresponds to a high local concentration of $Fe(CN)_6^{4-}$ above a single pore, indicating high ion flux. From SECM data, contours of constant $Fe(CN)_6^{4-}$ concentration above the pore were calculated and Eq. (3) was used to compute the absolute transport rate (mol/s) of $Fe(CN)_6^{4-}$ through the pore.

In the second stage of the experiment, the 0.1 *M* NaCl solution in the receptor compartment was replaced by a 0.01 *M* $FeCl_3$/0.1 *M* NaCl solution, and an iontophoretic current was applied for 60 min. The subsequent deposition of PB on the skin surface was documented by video microscopy. Figure 4B is an optical image of the same area of skin as that imaged previously by SECM in Fig. 4A. A blue dot has formed around the pore which was detected by SECM. The direct correspondence between skin pores imaged by SECM and those observed by PB staining demonstrates that the PB deposits act as reliable markers of locally high fluxes of $Fe(CN)_6^{4-}$.

The third stage of the experiment involved replacing the receptor compartment with 0.1 *M* NaCl. Transport rates through the same pores as in the first stage were then remeasured by SECM. The entire experiment was repeated for two skin samples. For the first sample, the initial stage (NaCl receptor) lasted ~5 hr. For the second sample, the initial stage lasted 23 hr. In each experiment, a constant current density of 40 μA/cm² was applied, and transport rates through four pores were individually measured both before and after PB formation.

Figures 5A and B show the transport rates through skin pores, for each of the two skin samples. In general, the transport rates were approximately equal before and after PB deposition. These data indicate that the formation of PB deposits on the stratum corneum had no significant effect on the transport rate of $Fe(CN)_6^{4-}$ through individual pores.

SECM was used in another experiment to investigate whether the time of a pore's activation (evidenced by the appearance of a PB dot) correlates with the apparent transport rate through it. From the videotape record of pore formation, the time at which pores had first appeared was noted. The receptor solution was then replaced with 0.1 *M* NaCl solution, and the relative transport rates of $Fe(CN)_6^{4-}$

A)

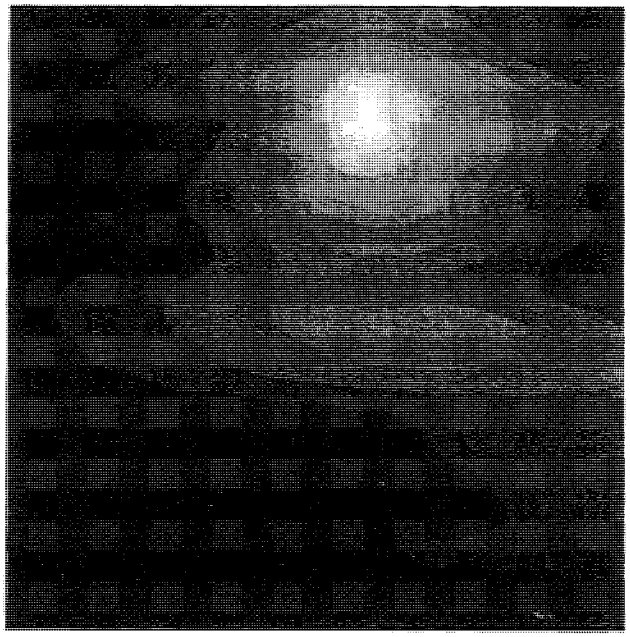

B)

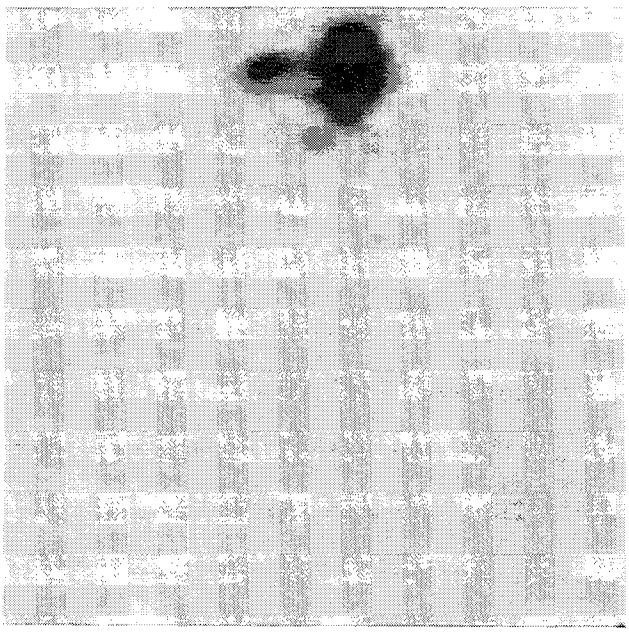

Fig. 4. (A) SECM image of $Fe(CN)_6^{4-}$ concentration over a 1-mm² region of hairless mouse skin during iontophoresis of $Fe(CN)_6^{4-}$ at j_{app} = 40 μA/cm². The bright area in A corresponds to high $Fe(CN)_6^{4-}$ above a skin pore. Donor solution: 0.1 *M* $K_4Fe(CN)_6$ (pH ~8.1). Receptor: 0.1 *M* NaCl (pH ~6.1). (B) Optical image of identical region of skin, recorded after deposition of PB at the pore opening.

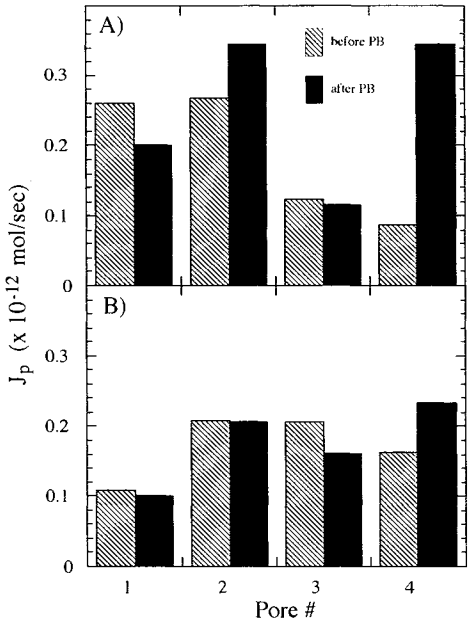

Fig. 5. Comparison of transport rate of $Fe(CN)_6^{4-}$ through individual pores, J_p, measured by SECM during iontophoresis (40 μA/cm²). Donor solution: 0.1 *M* $K_4Fe(CN)_6$. Receptor solution: 0.1 *M* NaCl. The transport rate through each pore was measured before and after 60 min of PB formation (see text). Data in A and B correspond to two different skin samples. (A) Skin sample subjected to approx. 5-hr initial iontophoresis prior to PB deposition. (B) Skin sample subjected to approx. 23-hr initial iontophoresis prior to PB deposition.

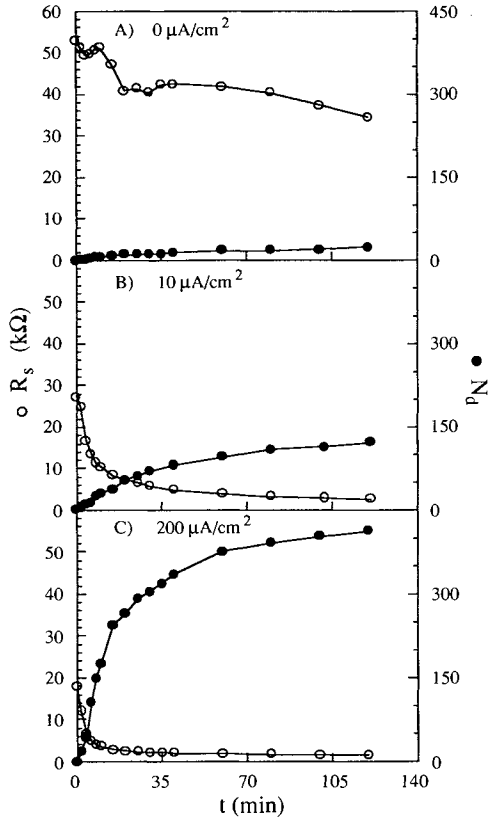

Fig. 6. Plots of skin resistance, R_s (○), and number of PB dots, N_d (●), vs elapsed time, *t*, for representative hairless mouse skin samples during iontophoresis at various current densities. Donor solution: 0.1 *M* $K_4Fe(CN)_6$ (pH ~8.1). Receptor: 0.01 *M* $FeCl_3$/0.1 *M* NaCl (pH ~2.2). (A) Sample 1, j_{app} = 0 μA/cm². (B) Sample 2, j_{app} = 10 μA/cm². (C) Sample 11, j_{app} = 200 μA/cm². Sample numbers correspond to numbers in Table I.

through 16 pores were measured by SECM. No correlation was found between the rate of $Fe(CN)_6^{4-}$ transport and the time of appearance of the pore.

In Fig. 2, some spatial clustering of dots is evident. Closer examination of video images revealed that these clusters often consist of groups of three or four dots in a line. A similar clustering of hair follicles was observed in optical micrographs of horizontal skin sections. Hair shafts were observed to protrude from ~3% of dots. Optical microscopy (20–40× magnification) of horizontal sections revealed that PB was deposited primarily on the stratum corneum surface. Very little PB was found within the tissue itself, although about 1% of hair follicles were found to contain PB. No visual evidence of holes, other than the hair follicles, was found in the dermis of skin samples after iontophoresis.

Correlation of Resistance Drop and Appearance of Pores. A strong correlation was observed between the total number of PB dots visible on the skin (N_d) and the skin resistance (R_s). In Fig. 6, the evolution of N_d and R_s is plotted for three representative samples at current densities (j_{app}) of 0, 10, and 200 μA/cm². The rate at which PB dots appear is initially large and decreases significantly after ~30 min. However, we did not observe a true steady-state value of N_d or R_s during the 120-min-long experiments. The PB deposits around each pore grew in size over time (Fig. 2). As the skin became covered with dots, the ability to observe the activation of new pores was impaired. This effect was most pronounced at the highest current density studied (200 μA/cm²), when the areal density of PB dots exceeded 600/cm².

In all experiments where current was applied (Figs. 6B and C), R_s decreased by a factor of 3–5 within the first 30 min and gradually leveled to a quasi-steady-state value at later times. Initial values of R_s ranged between 11 and 54 kΩ for 12 samples studied. This variability was likely due to biological variations between skin samples. The number of activated pores and the rate of change of R_s at earlier times (t <30 min) increased with increasing j_{app}. When j_{app} = 0, the decrease in R_s with time was insignificant in comparison to the large resistance drop observed when no current was applied. For instance, in Fig. 6A, R_s decreased by only 30% over a 120-min period.

Table I summarizes values of the total number of pores (N_d^f) and skin conductance (G_s^f) at the end of the experiment (~120 min) for 12 skin samples studied at current densities j_{app} ranging between 0 and 200 μA/cm². For j_{app} = 0 μA/cm², the passive flux of reactants was sufficient to form a small number of PB dots on the skin, but the number of dots increased dramatically when current was applied. The average density of pores (calculated by dividing N_d^f by the area of skin) observed after 120 min at the highest current density studied (200 μA/cm²) was 874 ± 138/cm², within the error of the average number of hair follicles (760 ± 150/cm²) counted by optical microscopy. This finding suggests that hair follicles may be the precursors of shunts.

A strong correlation was observed between the instan-

Table I. Conductivity Results for Hairless Mouse Skin

j_{app} ($\mu A/cm^2$)[a]	Sample no.	G_s^f ($\times 10^{-6}\ \Omega^{-1}$)[b]	N_d^f[b]	Linear region of G_s vs N_d plots[c] N_d (min)	N_d (max)	G_p[d] ($\times 10^{-6}\ \Omega^{-1}$)	G_b[e] ($\times 10^{-6}\ \Omega^{-1}$)
0	1	29.0	23	1	23	0.411	18.7
10	2	381.7	122	1	96	1.96	38
	3	84.0	57	1	50	0.936	8.76
	Average	230 ± 210	90 ± 46			1.45 ± 0.72	23 ± 21
40	4	80.7	121	6	121	0.381	40.1
	5	359.7	154	6	106	1.294	43.1
	6	123.0	84	6	84	0.914	36
	7	378.8	170	1	45	0.943	54.9
	8	190.1	111	13	111	1.13	49
	9	137.9	74	3	74	1.01	47.3
	Average	240 ± 130	119 ± 38			0.95 ± 0.31	45.1 ± 6.8
200	10	1890	385	0	369	2.11	81.1
	11	1475	412	0	412	1.39	49.6
	12	757.6	515	0	458	0.475	53.7
	Average	1370 ± 570	437 ± 69			1.33 ± 0.82	62 ± 17

[a] Iontophoretic currents are applied to skin samples using Ag/AgCl electrodes (see Fig. 1).
[b] G_s^f and N_d^f are the total skin conductance and number pores measured at the end of the experiment.
[c] The linear region of plots of skin conductance (G_s) vs number of pores (N_d) was determined by visual inspection.
[d] Average conductance of a pore (G_p) computed from slope of the linear region of G_s vs N_d plots [see Eq. (6)].
[e] Conductances of bulk skin tissue (G_b) calculated from the intercept of the linear region of G_s vs N_d plots [see Eq. (6)].

taneous skin resistance, R_s, and the number of pores observed by PB deposition. For instance, in Fig. 7, the resistance of a sample decreased rapidly for the first 5 min, then remained approximately constant over the next 10 min. At about 15 min, the resistance again began to decrease. The cause of the temporary plateau is not understood, but this data set illustrates the strong correlation between R_s and N_d. The appearance of several new pores immediately preceded the second decline in resistance at 15 min. The drop in resistance over the remainder of the experiment was accompanied by a continued increase in the number of pores. The appearance of PB dots immediately preceding the drop in resistance at 15 min suggests two things: (i) the decrease in skin resistance results from activation of a pores, and (ii) there is very little time lag between the activation of a pore and the deposition of a visible amount of PB at the site of the pore opening.

The data sets presented in Figs. 6 and 7 demonstrate

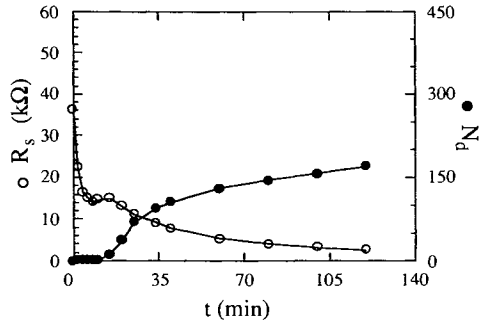

Fig. 7. (A) Plot of skin resistance, R_s, and number of dots, N_d, vs time, t, for sample 7, under experimental conditions similar to those in Fig. 6 (j_{app} = 40 $\mu A/cm^2$).

that the appearance of PB dots is accompanied by a decrease in the skin resistance. To quantify this relationship, we consider a simple model of the skin as a bulk phase containing a parallel network of pores. Let G_b represent the conductance of the bulk skin tissue, and G_{p_k} be the conductance of an individual pore. The total skin conductance G_s is given by Eq. (5).

$$G_s = G_b + \sum_{k=1}^{N_d} G_{p_k} \tag{5}$$

Assuming that the pore conductance G_{p_k} does not vary widely from pore to pore, the sum in Eq. (5) can be replaced by the product of N_d and the average conductance per pore (G_p) to give a simplified expression for the skin conductance.

$$G_s = G_b + N_d G_p \tag{6}$$

Using Eq. (6), values of G_p and G_b can be obtained from the slope and intercept, respectively, of a plot of G_s vs N_d (where G_s is simply $1/R_s$). In Fig. 8, the data from Fig. 6 is replotted as G_s vs N_d. For each sample, the plot is linear over a wide range of N_d. For a given sample, the linear region begins at low values of N_d, ranging from 0 to 13 pores. The linear behavior continues, in some samples, until the end of the experiment. In other cases, however, a sudden increase in the slope occurs at high values of N_d. This is illustrated most clearly by the data for samples 10–12, which were collected at 200 $\mu A/cm^2$ (Fig. 8D). In this graph, the plot of G_s vs N_d for sample 11 exhibits linear behavior over the entire range of N_d, while the slopes of curves for samples 10 and 12 increase sharply at N_d values above 350 and 480, respectively. An increase in the slope could be an indication that a new conduction mechanism (or mechanisms), other

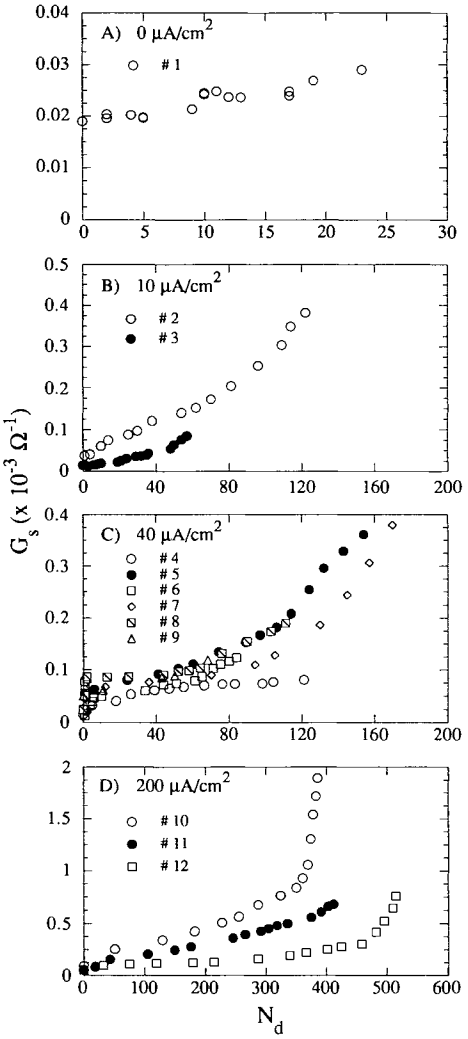

Fig. 8. Skin conductance, G_s, vs number of PB dots, N_d, plotted for samples 1–12, vs time, t, during iontophoresis at applied currents of (A) 0, (B) 10, (C) 40, and (D) 200 μA/cm².

than transport through uniformly sized pores assumed in Eq. (6), may be taking place. However, we believe that the abrupt increase in the slope results from dot-counting inaccuracies when the density of PB dots becomes so high that the ability to discriminate visually between pores is impaired. The clustering of pores contributes to the tendency to "hide" regions of skin where new pores may be forming but are not counted.

Table I lists values of G_p and G_b, computed from the slope and intercepts, respectively, of linear least-squares fits of G_s vs N_d. For each sample, the range of N_d over which the fit was made is also given in Table I. For current densities ranging from 10 to 200 μA/cm², average values of G_p varied from 0.945 to 1.448 × 10^{-6} Ω^{-1}. At j_{app} = 0 μA/cm² (sample 1), the calculated value of G_p is 0.411 × 10^{-6} Ω^{-1}, a factor of 2–3 lower than when a nonzero current was applied. However, within error, the value of G_p is found to be independent of j_{app}.

The measured valued of G_p can be compared to a crude estimation of the conductance of a hypothetical pore. The conductance of an ideal cylindrical "pore" filled with aqueous electrolyte can be estimated from Eq. (7):

$$G_p = \frac{\sigma \pi r_p^2}{l_p} \tag{7}$$

where σ is the electrolyte conductivity, and r_p and l_p are the pore radius and length, respectively. Although the conductivity within a skin pore is not known, we estimate it to be that of 0.1 M NaCl in aqueous solution: σ = 1.2 × 10^{-2} (Ω − cm)$^{-1}$. Assuming that the shunt pathways have radii and lengths of hair follicles, we estimate r_p = 23 μm and l_p = 350 μm [approximately half the thickness of "whole" hairless mouse skin (19)], yielding G_p = 5.7 × 10^{-6} Ω^{-1} from Eq. (7). This value is approximately three to five times greater than the mean experimental values listed in Table I. The agreement is remarkably close, given the simplicity of the cylindrical approximation.

As noted above, G_p appears to be independent of the applied iontophoretic current. This finding demonstrates that individual pores have an ohmic dc electrical response. However, the total number of pores (N_p) increases with the duration and the magnitude of current. Therefore, the total conductance of all pores, given by the product N_pG_p, is a function of time and current. For this reason, the skin, taken as a whole, has a nonohmic, time-dependent, dc electrical response.

Equation (6) does not account for the behavior of R_s before the appearance of the first pore. For instance, during the period between 0 and 10 min in Fig. 7, R_s drops by a factor of 2 even though no PB dots are visible by video microscopy. The decrease in R_s over this period may be due to the activation of pores which are not evident by PB staining or by an increase in the value of the bulk conductance (G_b). Such an increase may be related to initial equilibration with the chemical environment (e.g., hydration, ion exchange) in the early stages of the experiment. Although G_b may change significantly over the first few minutes of iontophoresis, a quasi-steady-state value is achieved within ~30 min, as evidenced by plateaus in plots of R_s vs t. The quasi-steady-state G_b, obtained from the intercept of plots of G_s vs N_d [see Eq. (6), Fig. 8, and Table I], increases very slightly with increasing j_{app} (Table I). This suggests that the conductance of the bulk pathway is weakly affected by the magnitude of the current.

The fraction of the total current carried by pores (f_p) may be calculated from Eq. (8).

$$f_p = \frac{N_d G_p}{G_s} \tag{8}$$

A value of f_p = 1 corresponds to all of the iontophoretic current passing through the pores. Figure 9 presents plots of f_p vs t for the 12 skin samples represented in Table I. At j_{app} = 0, f_p approaches a plateau value of 0.35. For j_{app} > 0, f_p increases rapidly from zero, approaching a peak or plateau value within the first 15 min. The maximum value of f_p at these currents ranges from 0.65 to 0.96. At later times the resistance either remains constant or decreases somewhat. The decrease in f_p is most dramatic for samples 10 and 12, which were studied at 200 μA/cm² (Fig. 9B). Mathemati-

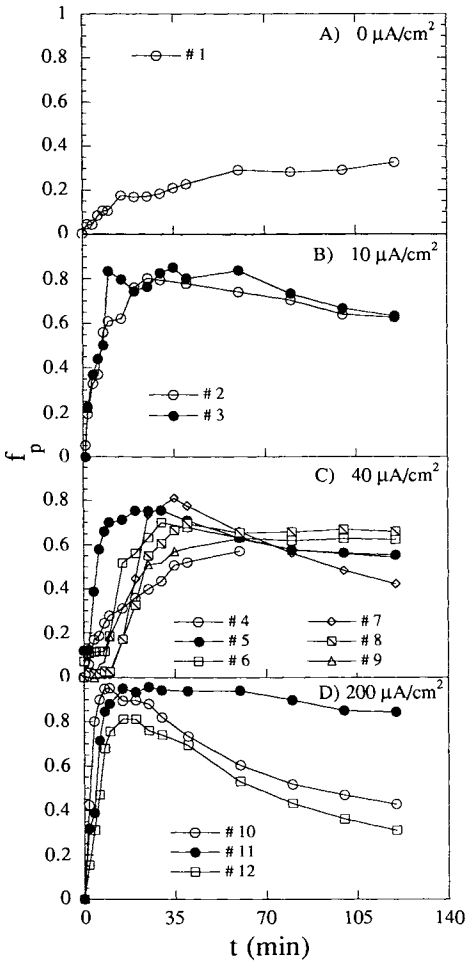

Fig. 9. Plots of fraction of total current which is carried by pores, f_p, plotted for samples 1–12, vs time, t, during iontophoresis at applied currents of (A) 0, (B) 10, (C) 40, and (D) 200 μA/cm².

cally, this effect is a direct result of the sharp increase in the slope of G_s vs N_d, which is observed for these samples (Fig. 8D) and is attributed to counting errors. In general, samples studied at current densities of 10 and 40 μA/cm² exhibited a value of f_p ranging from 0.6 to 0.7 after 60 min.

Effect of Chemical Environment. The above experiments were carried out in low-pH environments. It was impractical to perform this study with receptor solutions at normal physiological pH due to the decreased rate of the PB formation at higher pH values, as well as the tendency of aqueous Fe^{3+} to precipitate as $Fe(OH)_3$ at pH >3. Earlier in this paper, it was mentioned that the $Fe(CN)_6^{4-}$ transport rates measured at individual pores were approximately equal, both before and after a solution of 0.01 *M* $FeCl_3$/0.1 *M* NaCl (pH ~2.2) had been added to the receptor compartment of the iontophoresis cell for 60 min (Fig. 5). In order to explore the extent to which exposure of skin to this solution affected the total skin resistance, R_s was monitored for a sample before, during, and after it was subjected to 60 min of iontophoresis in a low-pH $FeCl_3$ solution. Figure 10A is a plot of R_s vs time made over a period during which the receptor solution composition and pH were varied. Open circles indicate R_s measurements made with a 0.1 *M* NaCl (pH ~6.1) receptor solution, and the filled circles represent data obtained with a 0.01 *M* $FeCl_3$/0.1 *M* NaCl (pH ~2.2) receptor solution. The initial R_s vs t profile in the initial (saline only) stage, from 0 to 300 min, has a shape similar to those of initial profiles obtained when the receptor contained $FeCl_3$ at low pH (Fig. 6). In the second stage, from 300 to 360 min, the addition of $FeCl_3$ to the receptor results in an increase in R_s, followed by an asymptotic decrease. After 60 min of iontophoresis in the second stage, R_s decreased to a value which was in close agreement with the valued measured immediately before the $FeCl_3$ was added. In the third stage, after 360 min, the value of R_s remains approximately the same as before the $FeCl_3$ exposure.

The number of PB dots (N_d) measured during the second stage of the experiment is plotted, along with R_s, in Fig. 10B. From these data, a plot of G_s vs N_d is shown in Fig. 10C. The relationship between the two parameters is similar in this experiment to results obtained for skin samples to which no previous current had been applied (Fig. 8A). Thus, the steady-state resistance is not significantly affected by the low-pH $FeCl_3$ solution.

During the second stage, the slope of the G_s vs N_d plot is $1.2 \times 10^{-6}\ \Omega^{-1}$, which is similar to the average values of

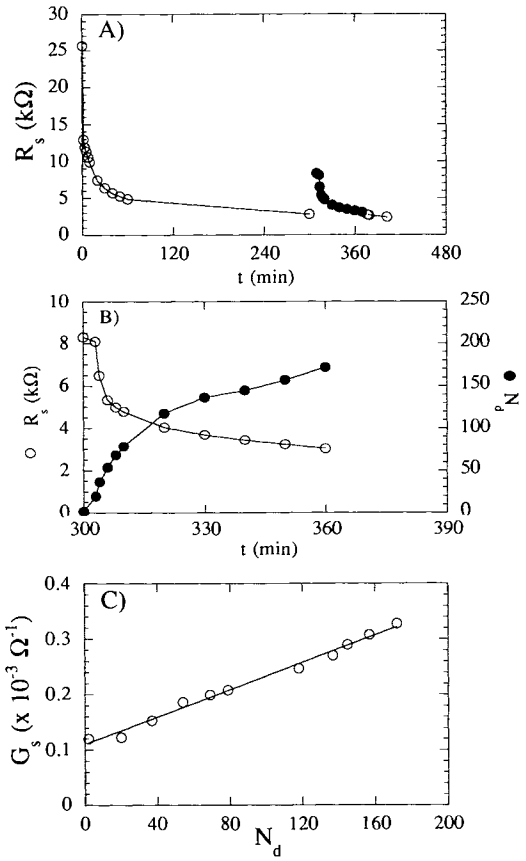

Fig. 10. (A) Plot of skin resistance, R_s, vs time, t, during iontophoresis of $Fe(CN)_6^{4-}$ at 40 μA/cm². The receptor contained 0.1 *M* NaCl (pH ~6.1) during the first 300 min and during the final 45 min (○). Between 300 and 360 min (●), 0.01 *M* $FeCl_3$/0.1 *M* NaCl was added to the receptor (pH ~2.2). (B) Plot of R_s and number of dots, N_d, vs time, t, while sample in A was exposed to $FeCl_3$. (C) Skin conductance, G_s, vs N_d calculated from data in B.

G_p listed in Table I. This result is consistent with the finding that the transport of $Fe(CN)_6^{4-}$, as measured by SECM, is not affected by the PB deposition process (Fig. 5).

Two events occurred between the first and the second stages of the experiment in Fig. 10A which may have resulted in the sudden increase in R_s at the start of the second stage: the iontophoretic current was interrupted for a period of ~10 min while the solution was changed in the receptor compartment; and the saline receptor solution was replaced by 0.1 *M* NaCl/0.01 *M* $FeCl_3$ (pH ~2.2). Whichever of these conditions triggered the transient skin response, it appears that the increase in R_s between the first and the second stages of the experiments may have resulted from a temporary reversal in the process which led to the original decrease in R_s in the first stage. If this is the case, the activation of pores may be a reversible process.

CONCLUSIONS

The formation of PB at sites of high counter-directional flux of $Fe(CN)_6^{4-}$ and Fe^{3+} allows direct visualization of conductive pathways in skin. The dye formation technique is different from dye residue techniques, in that the location of dye deposits is a direct indication of locally high transport rates, rather than the dye's binding affinity to various tissues.

The appearance of shunt pathways in hairless mouse skin is an activation mechanism, whereby a "latent shunt," which is inactive prior to iontophoresis, becomes activated through environmental factors, primarily the magnitude of applied current. One explanation for the current magnitude dependence is that local resistive heating may play a role in pore activation. However, it has been reported that heating of mouse skin does not significantly decrease its overall diffusional resistance for temperatures below ~70°C (30). The process may be reversible, which would explain the temporary increase in R_s observed in Fig. 10A. Reversibility of a pore's activation would indicate that the process of initial activation is not a result of removal of foreign or endogenous matter (e.g., soil or sebum) from a follicle. A mechanism for mechanical occlusion of sweat ducts, caused by swelling of the keratin surrounding the duct orifice, has been proposed by Randall and Peiss to explain the suppression of sweating in hydrated human skin (31). Mice have no eccrine sweat ducts, but swelling/shrinking of follicular structures in response to the chemical environment and/or application of current is conceivable.

The activation of pores correlates directly with a decrease in skin resistance. The conductance of pores was measured to be $0.936–2.11 \times 10^{-6}\ \Omega^{-1}$, independent of the current density in the range of 10 to 200 $\mu A/cm^2$.

The time dependence of the fractional contribution (f_p) of PB-stained pores to the total skin conductance varies during iontophoresis as a direct consequence of the activation of pores. For current densities of 10–200 $\mu A/cm^2$, f_p attains a maximum value of 0.6–0.95 within 5–30 min.

Using a physiologically based mathematical model, Scheuplein (14) stated that at times greater than 15 min, the majority of diffusional mass transport occurs overwhelmingly through the unbroken stratum corneum, due to the large fractional contribution of the stratum corneum to the total skin surface area, compared to that of the pores. Conversely, as a result of experiments done on the diffusion of ionic species across human cadaver skin, van Kooten and Mali concluded that 70% of transport occurs through sweat ducts (13). Our experimental results suggest that during constant-current iontophoresis across hairless mouse skin, pores initially contribute little to the total conductance, but within 5–30 min they are the primary routes of ionic transport.

The magnitude of applied current is the primary influence on the rate and number of pores which activate (open) during iontophoresis. However, the conductance of individual pores is not a function of the current. The opening of pores suggests that shunts result from activation of endogenous skin structures rather than from current-induced creation of artificial holes. The most likely precursors of shunts in hairless mouse skin are the hair follicles.

ACKNOWLEDGMENTS

The authors wish to thank Herbert Crandall (St. Paul Ramsey Hospital) and Dr. Elizabeth Rest and David Kist (Department of Dermatology, University of Minnesota) for tissue preparation and helpful discussions. This work was supported by a grant from Alza Corporation, Palo Alto, CA. A.I.L. gratefully acknowledges support from the NSF-Research for Undergraduates Program.

REFERENCES

1. T. Yamamoto and Y. Yamamoto. Electrical properties of the epidermal stratum corneum. *Med. Biol. Eng. Comput.* **14**:151–158 (1976).
2. A. van Boxtel. Skin resistance during square-wave electrical pulses of 1 to 10 mA. *Med. Biol. Eng. Comput.* **15**:679–687 (1977).
3. R. R. Burnette and T. M. Bagniefski. Influence of constant current iontophoresis on the impedance and passive Na^+ permeability of excised nude mouse skin. *J. Pharm. Sci.* 77:492–497 (1988).
4. W. I. Archer, R. Kohli, J. M. C. Roberts, and T. S. Spencer. Skin impedance measurement. In R. L. Rietschel and T. S. Spencer (eds.), *Methods for Cutaneous Investigation,* Marcel Dekker, New York, 1990, pp. 121–142.
5. A. K. Banga and Y. W. Chein. Iontophoretic delivery of drugs: Fundamentals, developments and biomedical applications. *J. Control. Release* 7:1–24 (1988).
6. G. B. Kasting and J. C. Keister. Application of the electrodiffusion theory for a homogeneous membrane to iontophoretic transport through skin. *J. Control. Release* 8:195–210 (1989).
7. H. A. Abramson and M. G. Engel. Skin reactions. XII. Patterns produced in the skin by electrophoresis of dyes. *Arch. Dermatol. Syphilol.* 44:190–200 (1941).
8. S. Grimnes. Pathways of ionic flow through human skin in vivo. *Acta Derm. Venereol.* 64:93–98 (1984).
9. R. R. Burnette and B. Ongpipattanakul. Characterization of the pore transport properties and tissue alteration of excised human skin during iontophoresis. *J. Pharm. Sci.* 77:132–137 (1988).
10. C. Cullander and R. H. Guy. Sites of iontophoretic current flow into the skin: Identification and characterization with the vibrating probe electrode. *J. Invest. Dermatol.* 97:55–64 (1991).
11. E. R. Scott, H. S. White, and J. B. Phipps. Direct imaging of ionic pathways in stratum corneum using scanning electrochemical microscopy. *Solid State Ion.* **53–56**:176–183 (1992).
12. R. T. Tregear. Relative penetrability of hair follicles and epidermis. *J. Physiol. (London)* **156**:307–313 (1961).
13. W. J. van Kooten and J. W. H. Mali. The significance of sweat-

ducts in permeation experiments on isolated cadaverous human skin. *Dermatologica* **132**:141–151 (1966).
14. R. J. Scheuplein. Mechanism of percutaneous absorption II. Transient diffusion and the relative importance of various routes of skin penetration. *J. Invest. Dermatol.* 48:79–88 (1967).
15. J. E. Wahlberg. Transepidermal or transfollicular absorption? In vivo and in vitro studies in hairy and non-hairy guinea pig skin with sodium (^{22}Na) and mercuric (^{203}Hg) chlorides. *Acta Derm. Venereol.* 48:336–344 (1968).
16. L. Brown and R. Langer. Transdermal delivery of drugs. *Annu. Rev. Med.* 39:221–229 (1988).
17. G. B. Kasting, E. W. Merritt, and J. C. Keister. An in Vitro method for studying the iontophoretic enhancement of drug transport through skin. *J. Membr. Sci.* 35:137–159 (1988).
18. T. Rosendal. Studies on the conducting properties of the human skin to direct current. *Acta Physiol. Scand.* 5:130–151 (1943).
19. R. L. Bronaugh, R. F. Stewart, and E. R. Congdon. Methods for in vitro percutaneous absorption studies II. Animal models for human skin. *Toxicol. Appl. Pharmacol.* **62**:481–488 (1982).
20. R. R. Burnette and T. M. Bagniefski. Influence of constant current iontophoresis on the impedance and passive Na^+ permeability of excised nude mouse skin. *J. Pharm. Sci.* 77:492–497 (1988).
21. B. Csillik, E. Knyihar-Csillik, and A. Squecs. Treatment of chronic pain syndromes with iontophoresis of vinca alkaloids to the skin of patients. *Neurosci. Lett.* **31**:87–90 (1982).
22. J. E. Sanderson, R. W. Caldwell, J. Hsio, R. Dixon, and R. R. Tuttle. Noninvasive delivery of a novel iontropic catecholamine: Iontophoretic versus intravenous infusion in dogs. *J. Pharm. Sci.* 76:215–218 (1987).
23. N. Harper, Bellantone, S. Rim, M. L. Francoeur, and B. Rasadi. Enhanced percutaneous absorption via iontophoresis I. Evaluation of an in vitro system and transport of model compounds. *Int. J. Pharm.* **30**:63–72 (1986).
24. B. Kari. Control of blood glucose levels in alloxan-diabetic rabbits by iontophoresis of insulin. *Diabetes* 35:217–221 (1986).
25. E. R. Scott, H. S. White, and J. B. Phipps. Measurement of iontophoretic transport through porous membranes using scanning electrochemical microscopy: Application to in vitro studies of ion fluxes through skin. *Anal. Chem.* (in press).
26. K. Sudeji, K. Furusawa, H. Inada, K. Katayama, M. Kakemi, and T. Koizumi. Enhanced percutaneous absorption of formoterol fumarate via pulsed iontophoresis. II. Effect of polarity, pulse frequency and duty. *Yakugaku Zasshi* **109**:771–777 (1989).
27. M. J. Pikal and S. Shah. Study of the mechanisms of flux enhancement through hairless mouse skin by pulsed DC iontophoresis. *Pharm. Res.* 8:365–369 (1991).
28. P. D. Gadsby. Visualization of the barrier layer through iontophoresis of ferric ions. *Med. Instrum.* **13**:281–283 (1979).
29. K. Honda, K. Chiba, and H. Hayashi. Polymerization of transition metal complexes in solid polymer electrolyte membranes. *J. Macromol. Sci. Chem.* **A26**:609–620 (1989).
30. R. O. Potts. Physical characterization of the stratum corneum: The relationship of mechanical and barrier properties of lipid and protein structure. In J. Hadgraft and R. H. Guy (eds.), *Transdermal Drug Delivery. Developmental Issues and Research Initiatives,* Marcel Dekker, New York, 1989, pp. 23–57.
31. W. C. Randall and C. N. Peiss. The relationship between skin hydration and the suppression of sweating. *J. Invest. Dermatol.* **28**:435–441 (1957).